This is a repository copy of *Low-profile independently- and concurrently-tunable quad-band antenna for single chain sub-6GHz 5G new radio applications*.

Article:

Low-Profile Independently- and Concurrently-Tunable Quad-Band Antenna for Single Chain Sub-6GHz 5G New Radio Applications

SAJID M. ASIF[1], (Member, IEEE), MOHAMMAD R. ANBIYAEI[2], (Member, IEEE), KENNETH L. FORD[1], (Senior Member, IEEE), TIMOTHY O'FARRELL[1], (Senior Member, IEEE), AND RICHARD J. LANGLEY[1], (Senior Member, IEEE)

[1]Department of Electronic and Electrical Engineering, The University of Sheffield, Sheffield S1 4ET, U.K.
[2]Faculty of Engineering, Alzahra University, Tehran 19938 93973, Iran

Corresponding author: Timothy O'Farrell (t.ofarrell@sheffield.ac.uk)

ABSTRACT This paper presents a quad-band frequency agile antenna, with independent and concurrent frequency tunability in each band, for a tunable, concurrent, quad-band single chain radio receiver for 5G New Radio (NR). More specifically, the antenna comprises of four planar slots etched in a ground plane and fed through a single microstrip feedline, without any impedance matching network. The structure is optimized to maximize isolation between the individual slots and their respective resonant frequencies. Furthermore, a novel high order harmonic suppression method is demonstrated, which controls the current distribution via creating a fictitious short circuit in the slot antenna–enabling the antenna to achieve a much wider tuning range. Numerical simulations are verified using experimental implementation and measurements, with good agreement observed. The four slots resonate around the 830 MHz, 1.8 GHz, 2.4 GHz and 3.4 GHz frequency bands, which are independently tuned (using a varactor diode in each slot) to achieve tuning ranges of approximately 64%, 66%, 27% and 33%, respectively. More importantly, the contiguous four bands covers a total frequency tuning from 0.6 to 3.6 GHz i.e. a tuning range of approximately 143%. Finally, far-field measurements are performed and the antenna is evaluated in over-the-air testbed (quad-band radio receiver), which measures the Error Vector Magnitude performance for the individual channels. Good performance is observed, confirming acceptable isolation performance between the four bands. The data reported in this paper is available, from ORDA-The University of Sheffield Research Data Catalogue and Repository, at https://doi.org/10.15131/shef.data.11219000.v1.

INDEX TERMS Multiband tunable antennas, reconfigurable antennas, frequency agility, reconfigurable radio receivers, agile 5G communication systems, cellular radio.

I. INTRODUCTION

5G is the next generation of mobile and wireless technology, capable of providing ultrafast speeds, low latency and much greater reliability. It is expected that while operating across a wide range of frequencies, the new 5G Radio Access Networks (RANs) will support multiple simultaneous connections, for example, concurrent communication of a device

The associate editor coordinating the review of this manuscript and approving it for publication was Qammer Hussain Abbasi.

with multiple network nodes [1]–[3]. A common solution would be a multi-chain communication system; however, such a system would increase the size, complexity and cost as well as the power consumption of a handset. Alternatively, a single chain transceiver system with multiband concurrent Frequency Agile Radio (FARAD) system, as shown in Fig. 1, can provide a compact and power efficient solution for future 5G RANs [4], [5].

Thus, the RF-front end of the mentioned FARAD system would require the antennas to be frequency agile and
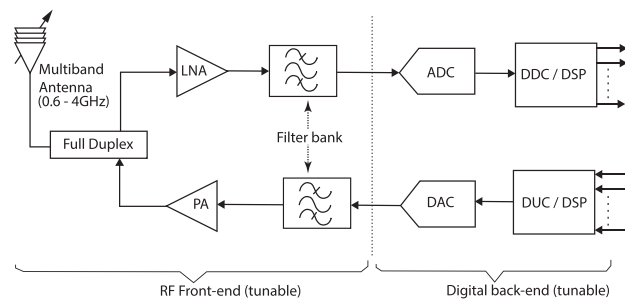
FIGURE 1. A general system-level diagram of the Frequency Agile Radio (FARAD) showing the tunable RF front-end and digital back-end.

support multiple frequency bands concurrently and, more importantly, the independent tuning of resonant frequency bands across the operating frequency range. Frequency agile antennas (FAA), with multiband tuning capability, can be designed on low-cost printed circuit boards, which is the main consideration for handheld and mobile wireless devices, and is the focus of this work. The FAA is a subcategory of the reconfigurable antennas, including pattern- and polarization-agile antennas, which employs the following methods to achieve the reconfigurability: Mechanical actuation (electromechanical, piezoelectric, micro-actuators etc.); Tunable materials (bulk semiconductors, ferroelectrics, liquid crystals etc.); and Integrated Electronic Devices (PIN diode Switches, MEM switches, Varactor diodes etc.). Over the past two decades, numerous configurations of FAA have been considered, where different tuning methods have been integrated with various antenna types such as printed dipoles, planar inverted-F antennas, microstrip patches, slot antennas, and dielectric resonator antennas (etc.). A comprehensive overview of these configurations as well as details about the tuning techniques is reported in [6]–[8]. While each mentioned reconfigurable and tuning technique has its own merits and demerits, the integration of a discrete electronic component in a low-profile antenna is desired for a handset or mobile application.

Contrary to the multiband antennas with fixed frequency bands [9], the frequency reconfigurable antennas provide the flexibility to support new services; these latter antennas may be categorised into discrete and continuous tuning antennas. PIN diodes are mostly used to achieve discrete tuning as their switching states allow the switching of the resonant frequencies [10]–[15]. For continuous tuning, varactor diodes are mostly used as they enable the antennas to have a smooth transition between the operating frequencies [17], [19], [21], [23]. All the antennas reported in [10] to [19] using these techniques are limited to a single or dual-bands. Researchers have been using various techniques to achieve the independent tunability of multibands over wide ranges. For example, Behdad *et al.* achieved a tuning range of 2.02 GHz with a dual-band reconfigurable antenna, which measured 110×150 mm^2 [19]. Also, Song *et al.* proposed a two-port dual-band reconfigurable chassis antenna with a wide tuning range of 2.1 GHz; however, it was of high-profile

and needed an external matching network [24]. Recently, a quad-band antenna with independent tunability has been presented but the independent tunability is dependent upon changing the physical parameters and also requires an additional matching network [25]. In [21], our related work on a tri-band slot antenna was reported where three independent frequency bands were tuned to achieve a tuning range from 0.6–2.7 GHz, but extending the tuning range beyond 2.7 GHz remained an issue due to the higher order resonant modes of the first frequency band.

The aforementioned limitation of the slot antenna is addressed in this paper. In particular, the higher order resonant modes of the slot antenna are suppressed by creating a fictitious short circuit in the radiating structure, which controls the surface currents and enables the proposed slot antenna to have a much wider tuning range of $\approx$143%, reported for the first time. This mentioned method is demonstrated using a quad-band varactor-loaded slot antenna, the resonances of which can be independently and/or concurrently tuned to achieve a tuning range from 0.6 to 3.6 GHz. The proposed antenna has a planar structure with four varactor-loaded slots in the ground plane, which allows continuous tuning of the resonant frequencies upon reverse biasing. All the slots are fed using a single 50 Ω microstrip line, the design of which is optimized to provide the necessary matching over the entire bandwidth of 3 GHz, without any feeding network. All the modeling, simulation and optimisation is carried out using a full-wave 3D simulation software, CST Studio Suite (ver. 18.0). The final antenna design is fabricated and measured to validate the concept. Following the performance measurements of the prototype antenna, which showed good agreement with the simulation results, the antenna is tested and validated in an over-the-air testbed for a quad-band, concurrent, single chain radio receiver for sub-6GHz 5G NR – which is demonstrated for the first time.

This paper is organised as follows: Section II describes the operating principle and the design technique of the proposed quad-band loaded-slot antenna and explains the numerical modeling and simulations. The details of the antenna prototype are given in Section III while the results are presented in Section IV. Finally, the discussions and conclusions are summarized in Section V and VI, respectively.

II. ANTENNA DESIGN
The aim of this work is to design a low-profile quad-band antenna with independent and concurrently tunable bands for single chain radio receiver for 5G NR(New Radio). Contrary to a wideband antenna, the proposed narrow band antenna with independent controllability of bands has a competitive advantage as it eliminates the need of additional filters required for cancelling the unwanted noise and hence offer better RF stability. There are other low-profile antennas available to explore for frequency tuning, yet we selected slot antenna specifically because multiple slots can be excited using a single microstrip feed-line without needing any
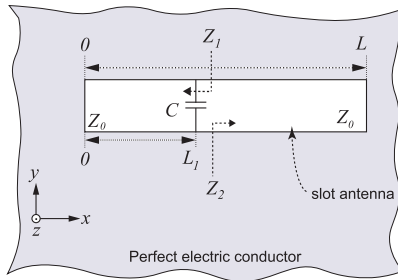
FIGURE 2. The transmission line model of a loaded-slot antenna in a large perfect electric conductor. Z_0 is the slot line impedance; L_1 is the capacitor's location; C represents the capacitance in the slot; Z_1 and Z_2 are the input impedances to the left and right of the reference point; L is the length of the slot.

FIGURE 3. Design evolution of the frequency agile quad-band antenna, with planar structure. A single-, dual-, tri-, and quad-band antennas are shown in (a), (b), (c), and (d), respectively. Bottom layer shows the microstrip line (feed) while top layer is the ground plane.

additional matching network. This property provides an enhanced flexibility and significantly simplifies the over-all design of a tunable slot and its feed network, resulting in low complexity and high reliability for multiband slot antenna. Contrary to other antennas (e.g. dipoles), which requires a specially designed matching network, this feature of the slot antenna makes it appealing for reconfigurable or tunable applications especially when multiband tunability is desired [15].

A. THEORY OF LOADED-SLOT ANTENNAS

A slot antenna, at its fundamental resonance, can be considered as a $\lambda/2$ transmission line, when short circuited at both ends [26], [27]. The loading of a slot with a capacitor, as shown in Fig. 2, results in the increase of the line capacitance at one particular point and consequently reduces its fundamental resonant frequency and all its higher-order resonances. However, this reduction is non-uniform and determined by the capacitor's location (L_1), capacitance and the slot line impedance (Z_0). The resonant frequency of the the loaded-slot can be determined by the transmission line equivalent circuit model [19], as illustrated in Fig. 2. More specifically, by applying the tansverse resonance condition [28], [29], the equation for the resonant frequencies of this loaded-slot (Fig. 2) can be written as,

$$\tan \beta L_1 + \tan \beta (L - L_1) - \omega C Z_0 \tan \beta L_1 \tan \beta (L - L_1) = 0 \tag{1}$$

where β is the propagation constant (frequency dependent), C is the capacitance and ω is the angular frequency. Eq. 1 can be solved numerically as a function of frequency, capacitance value and its position (L_1) to obtain the resonant frequencies of the loaded slot, as reported in [30]. It should be noted that the effect of the antenna feed is not considered in this model, which does affect the antenna's resonant frequencies.

The mentioned operating principle is used for the approximation of the resonance frequencies of the proposed antenna and numerical simulations were performed for the complete evaluation. More specifically, four varactor-loaded slots were used, as separate radiating elements, to achieve the frequency range from 0.6 to 3.6 GHz.
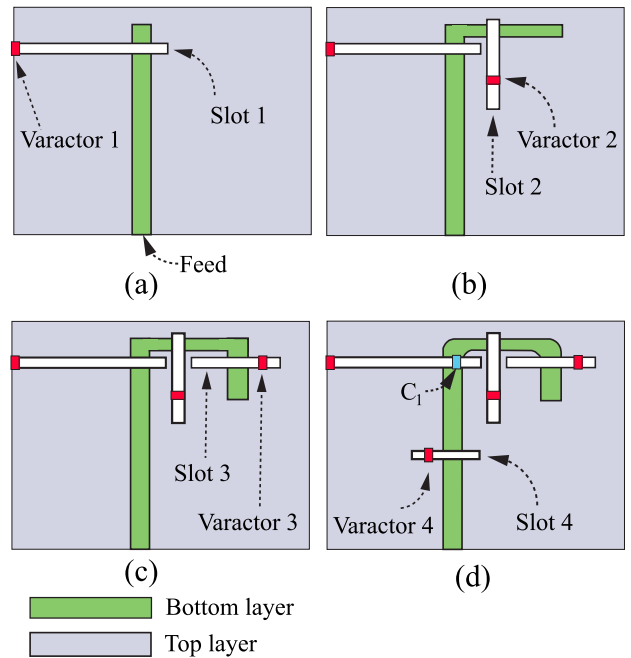
B. ANTENNA GEOMETRY AND DESIGN EVOLUTION

The design evolution of the proposed quad-band antenna comprising of a ground loaded with four slots and a microstrip feed, on a planar structure, is shown in Fig. 3. The respective antenna layouts in Fig. 3(a-d) illustrate the design procedure of the proposed quad-band antenna. More specifically, the antenna consists of four slots separately designed on a common ground plane on a double-sided 1.524 mm thick Rogers TMM4 substrate with a dielectric constant $\epsilon_r = 4.5$ and loss tangent $\tan \delta = 0.002$. The final parameters of the antenna are shown in Fig. 4. Each slot is designed separately, to achieve the desired resonant frequency, using the design techniques mentioned in the previous sub-section. The standard microstrip feed-line is used to excite the slot antennas but it is important to note that at each feeding point the input impedance is a function of frequency. Typically, to obtain a good 50 Ω matching the feed-line is moved close to an end of the slot but any change in the electrical length also affect the impedance match and hence need to be carefully optimized using numerical methods [15]. It should be noted that with the incorporation of additional feed-lines for subsequent slots, any discontinuity in the feed-line has to be compensated by the feed position and varying electrical length.

The design steps of the proposed quad-band antenna can be described with the help of Fig. 3(a) to (d), as follows:

Step 1: A single slot (slot 1) is designed to achieve a resonant frequency in the sub-GHz region and then the slot dimensions and feed position was optimized to integrate a
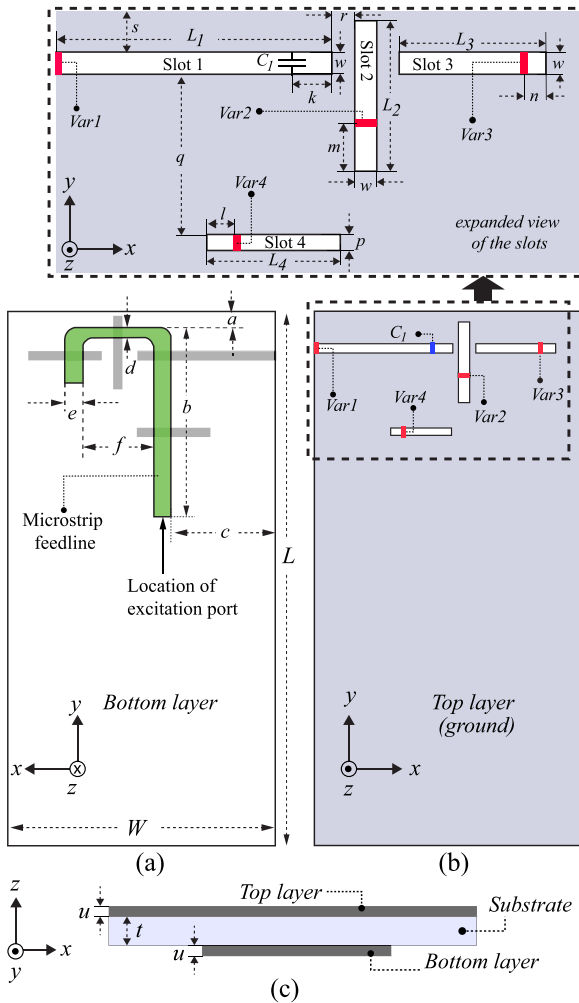
FIGURE 4. Antenna geometry. (a) Bottom layer, showing the excitation position and microstrip line (feed). (b) Top layer with details of the four slots and the positions of the varactor diodes (Var1-Var3 = Varactor diodes, Infineon BB833; Var4 = Varactor diode, Skyworks SMV 1405; C_1 = 1 pF (RF, high-Q)). Dimensions are (in mm): W = 50, L = 100, a = 3.0, b = 35.0, c = 19.9, d = 2.0, e = 3.2, f = 13.3, r = 1.0, s = 6.0, q = 12.65, L_1 = 26.0, L_2 = 15.5, L_3 = 15.0, L_4 = 11, w = 2.0, k = 4.0, $m = n$ = 3.0, p = 1.0, l = 2.09, u = 0.0175 and t = 1.524.

FIGURE 5. Simulated current distribution of the slot-loaded ground plane at the (a) higher order mode (HOM) resonance, and (b) when the HOM resonance is suppressed.

varactor diode to achieve the frequency tuning from 0.6 GHz to 1.17 GHz.

Step 2: In order to extend the frequency tuning range beyond 1.17 GHz, a second slot (slot 2) was added in the orthogonal position to the slot 1, with a separation of 2 mm, and furthermore, the microstrip feed line was extended to excite slot 2 to achieve a second resonant frequency band at around 1.17 GHz. Furthermore, a varactor diode was added to this slot and the feed position was optimized to attain good impedance matching for the second band tuning from 1.17 GHz to 2.2 GHz.

Step 3: Next, to extend the frequency range of the proposed antenna beyond 2.2 GHz, we achieved a third frequency resonance by introducing a third slot (slot 3), parallel to the x-axis and orthogonal to slot 2. The microstrip feed line was extended, with a 90° discontinuity, to provide the necessary
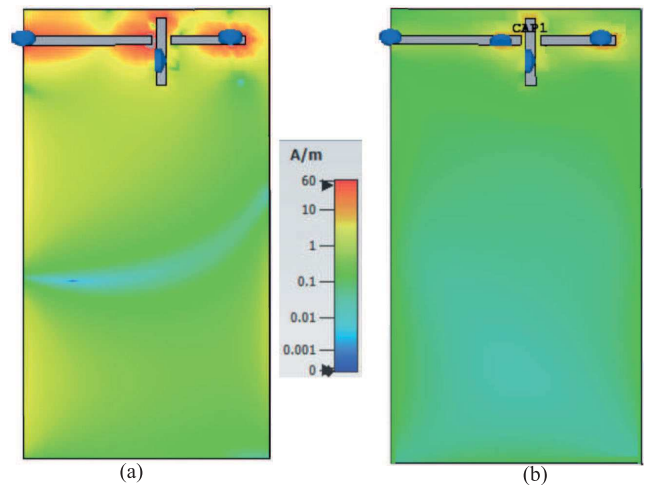
excitation to slot 3, and furthermore, a varactor diode was added in the appropriate position to tune the third frequency band, achieving a tuning range from 2.2 GHz to 2.7 GHz.

Step 4: In order to extend the frequency range of the proposed antenna (beyond 2.7 GHz), a fourth slot had to be introduced but first, the higher order mode (HOM) resonance produced above 2.7 GHz had to be suppressed. In Fig.5(a), the current distribution of the proposed antenna, with three-slots, at 3.1 GHz can be observed, which is indicative of the HOM resonance, as further depicted in the results (Fig. 6). These HOM resonances must be cancelled to achieve a tuning range beyond 2.7 GHz. Previously, in [16], a concept of fictitious short circuit was employed to change the bandwidth characteristics of a slot antenna. The same concept was adapted to manipulate the currents on the slot-loaded ground plane of the proposed antenna using a small capacitor (1pF; CAP1) at a particular location in slot 1, as shown in Fig. 5(b). The uniform current distribution (Fig. 5(b)) is indicative of the fact that the HOM resonances are fully suppressed, which is achieved using numerical simulation. More specifically, the numerical characterisation of this concept revealed that a 1 pF capacitor, placed at a distance of 4 mm from the slot's edge (right-hand side), would suppress the unwanted HOM resonance. These results were experimentally validated using a prototype antenna and are shown in Fig. 6. It can be observed that the correct capacitance value (C_1 in Fig. 3(d)) is critical not only for the suppression of the HOM resonance, but also to maintain the three fundamental resonances (B1 to B3), as shown in the comparison study in Fig. 6.

The suppression of the aforementioned HOM resonance enabled the remaining frequency spectrum (3 GHz - 4 GHz) to be used for extending the overall tuning range of the proposed antenna.

Step 5: Finally, the tri-band antenna design, shown in Fig. 3(c), was exploited to achieve an additional resonance to ensure that the overall antenna design remains compact
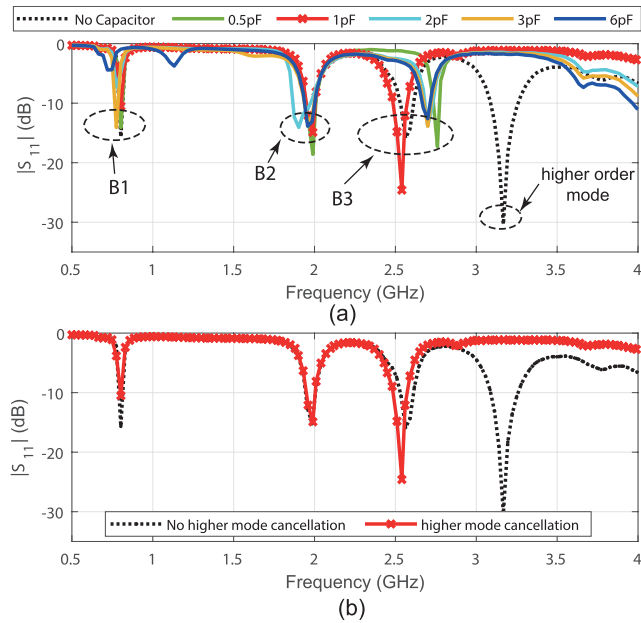
(a)

(b)

FIGURE 6. A comparison of the reflection coefficients ($|S_{11}|$ in dB) of the tri-band antenna. (a) Effect of the capacitor and its values on the first three bands (B1, B2 and B3) and the higher order mode resonance. (b) Final results of the tri-band antenna with (1 pF capacitor) and without (no capacitor) the cancellation of higher order mode resonance.

and meets the mobile handset size restrictions. Employing the existing microstrip feed, a fourth slot (slot 4) was introduced at an appropriate position to achieve an additional resonance to allow the frequency tuning to be extended beyond 2.7 GHz. Oriented in the x-axis, this slot was separated by a distance, q, of 12.65 mm from slot 1. Through full-wave simulations, it was observed that reducing the distance q affects the impedance matching of the fourth band. For example, by changing q from 12.65 mm to 10.15 mm, the value of $|S_{11}|$ (of the fourth band) was reduced from -20 dB to -6 dB respectively. Further reduction in q (< 10.15 mm) resulted in a complete mismatch of the fourth frequency band.

Furthermore, the bends in the microstrip feed line were chamfered (Fig. 3(d)) to compensate the excess capacitance and improve the overall impedance matching [31]. The varactor-loaded fourth slot measures only 11 mm×1.0 mm and results in extending the tuning range of the proposed antenna to 3.6 GHz. Fig. 6 shows the reflection coefficients of the first three bands, however, complete results of the tuning ranges of each band are presented in Section IV.

C. NUMERICAL MODELING AND SIMULATION
The numerical modeling and simulation of the antenna was performed using the EM/Circuit Co-simulation technique in CST Design Studio (Microwave Studio and Circuit Studio), where, for simplicity, the varactor diodes were initially modeled as variable capacitors. Next, to add a more realistic model of the varactor diode, each variable capacitor was replaced with a Discrete Port and simulations were performed. The complete simulated model was then imported
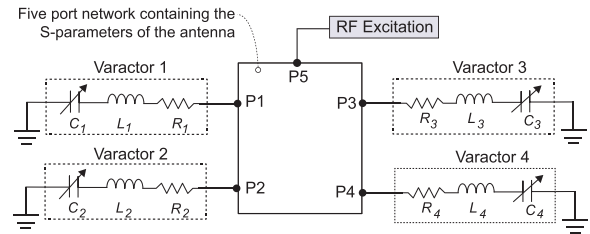

FIGURE 7. Schematic of the antenna and equivalent circuit model of varactor diodes used in the co-simulations. Varactor 1 to 3 are Infineon BB833 ($R_1 = R_2 = R_3 = 1.8\,\Omega$, $L_1 = L_2 = L_3 = 1.8nH$, C_1 = voltage dependent which varies from 0.6pF (30V)-10pF (0V). Varactor 4 is Skyworks SMV1405 ($R_4 = 0.8\Omega$, $L_4 = 0.7nH$, C_4 = voltage dependent which varies from 0.63pF (30V) to 2.67pF (0V).

into the CST Circuit Studio environment and the equivalent circuit model of the varactors were connected to the designated Ports and circuit simulations were performed to incorporate the circuits (equivalent model of varactors) with the antenna model. Finally, the EM/Circuit Co-simulations were completed to study the S-parameters and far-field characteristics of the proposed antenna.

As shown in Fig. 7, the equivalent model of the varactor diodes comprises of serially connected *RLC* lumped elements i.e. series resistance R, inductance L and junction capacitance C. This simplified model is known for the biasing of active antennas [32], [33]; however, it neglects the parasitic components which are often considered for high-frequency microwave applications e.g. the distributed line package model and capacitance due to ground proximity. For the sub 3 GHz frequency tuning (slots 1-3), the Infineon BB833 varactor diode was chosen due to its high capacitance ratio and reliable performance [21], [34]. However, for frequency tuning above 3 GHz, the Skyworks SMV1405 was used (in the 4th slot), which features high-Q and low-series resistance [35].

D. CURRENT DISTRIBUTION
The surface current distribution of four slots was investigated to examine the working mechanism of the proposed antenna. The surface current distribution of slots 1, 2, 3 and 4 when resonant at the frequencies of 0.83, 1.8, 2.4 and 3.4 GHz are depicted in Fig. 8(a)-(d), respectively. The operating characteristics of each slot can be graphically observed from the presented current distribution. For example, it is observed in Fig. 8(a) that strong currents are only present around slot 1, which resonates at the lower end of the proposed spectrum (820 MHz). Furthermore, Fig. 8(b) and (c) shows the current density around slots 2 and 3, respectively, the radiation of which contributes to the second and third frequency bands (1.8 GHz and 2.4 GHz). It can be observed that slot 1 and 3 are in line with each other, a parallel configuration, which is reported to generate additional resonances and may well influence the independent tunability of these slots. Thus, slot 2 is placed orthogonally between slots 1 and 3 to reduce the potential unwanted coupling, as the EM fields of slot 2 is cross-polarised to those of slots 1 and 3. Fig. 8(d) shows
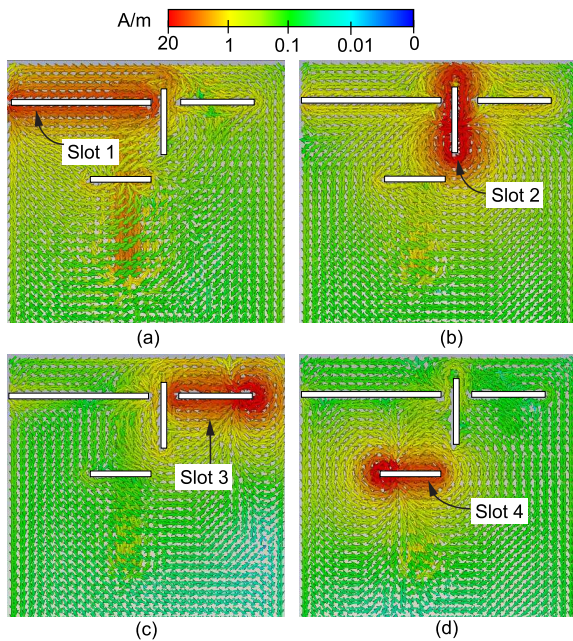
FIGURE 8. Current distribution at the resonant frequencies of: (a) 820 MHz, (b) 1.8 GHz, (c) 2.4 GHz, and (d) 3.4 GHz, produced by the first, second, third, and fourth slot, respectively.

strong currents only around slot 4, which contributes to the resonance of the 4th frequency band (3.4 GHz) and further illustrates that the currents are uniformly distributed around the other slots.

E. BIASING CIRCUIT

In order to realise a practical working prototype, the biasing circuit for each varactor diode was designed on the same printed circuit board. A schematic diagram of the circuit, designed for biasing each varactor diode, is shown in Fig. 9(a). Initially, a U-shaped slot was created around each varactor's cathode terminal to isolate the RF and DC, as shown in the illustration of modifications to slot 3 in Fig. 9(b). The two parallel capacitors C_5, placed in the U-slot, allows RF continuity while acting as an open circuit for the DC current path. The via (shown in Fig. 9(b)), however, connects the varactor diode to the remaining DC biasing circuit on the bottom layer of the PCB, as illustrated in Fig. 9(c). More specifically, in this example, the via (Fig. 9(b)) connects the varactor's cathode terminal to the RF choke L_{C3}, which provides the necessary RF-DC isolation i.e. choking the RF while allowing the DC current to flow. Furthermore, thin microstrip lines (0.2 mm) are created for each biasing circuit, which not only provides the path for DC current but also results in an additional inductance in series with the inductance of the RF choke. Overall, four separate DC power supplies (indicated as V_1, V_2, V_3 and V_4) provide biasing to the four varactor diodes using four separately designed isolated biasing circuits. In order to facilitate the experimental measurement process, a low-impedance 5×5 mm pad was created (using multiple vias) on the same layer to provide a common ground for DC biasing.
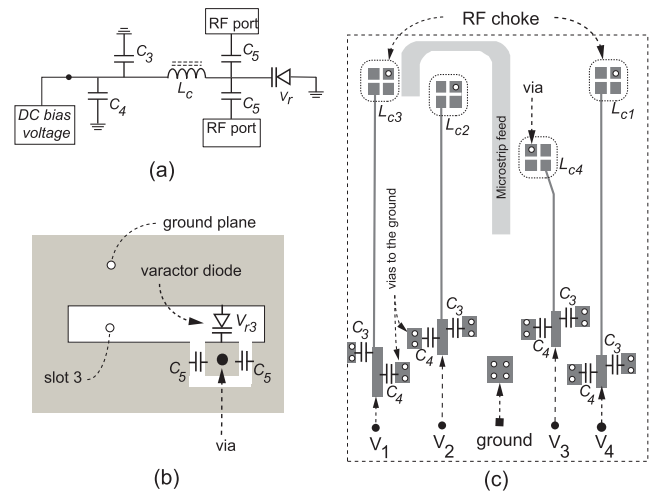

FIGURE 9. Details of the biasing circuit. (a) A schematic of the biasing circuit with all the components used for biasing the varactor diodes. (b) Illustration of additional slots created to incorporate the biasing lines and provide necessary isolation. (c) Illustration of additional pads, vias and microstrip lines to complete the biasing circuit (Figure is not drawn to scale).

As per Fig. 9(c), the four RF chokes are denoted as L_{C1}, L_{C2}, L_{C3} and L_{C4} whereas C_3 and C_4 are the capacitors used to help filter off any RF leaking through the choke on to the DC power supply line, and to short out any low frequency noise or spurs on the power supply so that they do not pass through the choke and get into the radiating slots. Finally, the modified antenna was re-simulated and the resultant changes in the frequency resonances were minimized by further adjustment of the antenna parameters (Fig. 4).

F. EFFECTS OF VARACTOR'S LOCATION ON RESONANT FREQUENCY

The approximate transmission line model of a loaded-slot antenna, as summarised in Section II(a), acts as a design tool to determine the resonant frequency of a slot antenna for a given value and location of the capacitor in the slot. It is worth noting that the aforementioned method, also extensively studied in [19], [30], is only an approximation of the real resonant frequency of the actual antenna because the effects of radiation (from the slot antenna) and moreover the effects of the feed network parameters on the antenna's resonant frequencies are ignored. For accurate prediction of the actual resonant frequency of a slot antenna, full-wave simulation is used, which considers the effects of the finite ground plane, dielectric substrate, radiation, and especially the feed network parameters on the resonant frequency of the antenna. A separate comparison study where both methods, analytical and full-wave simulation, which have been used to predict the resonant frequencies reported a maximum error of up to 8% [30]. Besides, it is observed that the feed location equally plays an important role in achieving and maintaining a good impedance matching. For example, by changing the location of the varactor diode, Var1, in slot 1 (Fig. 4(a)) and moving it away from the edge of the board or towards the
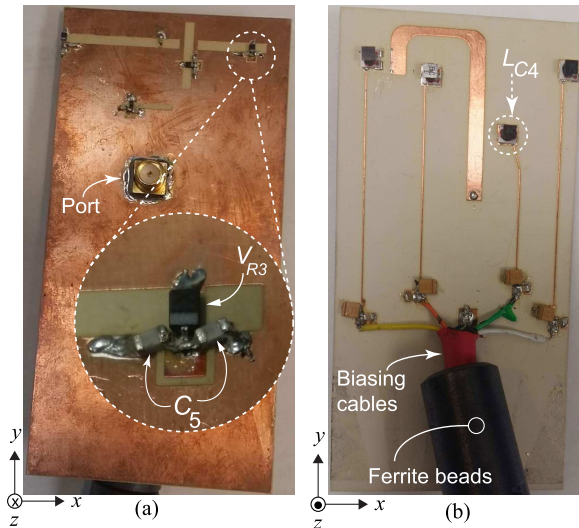
FIGURE 10. Pictures of the manufactured prototype quad-band frequency agile antenna showing (a) top layer (C_5 is the DC blocking capacitor, V_{R3} is the varactor diode in the third slot) and (b) bottom layer (L_{C4} is the RF choke (TCCH-80+)).

TABLE 1. Details of the components.

Component Type	Symbols	Details
Varactor Diode	V_{R1}, V_{R2}, V_{R3}	Infineon BB833
Varactor Diode	V_{R4}	Skyworks SMV1405-079
RF Choke	$L_{C1}, L_{C2}, L_{C3}, L_{C4}$	Mini-circuits TCCH-80+
Capacitor	C_5	100 pF (RF, high Q)
Capacitor	C_3, C_4	39 nF, 1 μF (TANT)

on the PCB to check for any errors in the assembly and fabrication. Moreover, to connect the fabricated prototype to DC power supplies, the DC-biasing lines were screened (using a thin conducting foil) and passed through ferrite core sleeves to provide shielding and reduce any unwanted EM radiation. Details of the components is provided in Table 1, while a picture of the final prototype antenna is shown in Fig. 10.

IV. MEASURED RESULTS
A. REFLECTION COEFFICIENTS AND TUNING RANGE
The input reflection coefficients or the $|S_{11}|$ (in dB) of the prototype antenna were measured in an anechoic chamber with a calibrated Vector Network Analyser, Agilent E5071C. During these measurements, the four varactor diodes were reverse biased using four separate digital power supplies (0–30V), as indicated by V_1, V_2, V_3, and V_4 in Fig. 9(c). All four biasing voltages were applied concurrently to study the full tuning range of the antenna; however, only one biasing voltage was varied at a given time to investigate the tuning range of that specific frequency band. To study the frequency tuning of the first band, the bias voltage (V_1) of the first varactor diode V_{R1} was varied while the bias voltages (V_2 to V_4) of the remaining varactor diodes (V_{R2} to V_{R4}) were kept constant to achieve the fixed second, third and fourth resonant frequencies. As shown in Fig. 11, the achieved $|S_{11}|$ (-6 dB) tuning range of the first band covers frequencies ranging from 600 MHz to 1.17 GHz, while the second, third, and fourth frequencies were fixed at 1.85 GHz (@8.68 *V*), 2.4 GHz (@12.4 *V*) and 3.4 GHz (@9.3 *V*), respectively. This first tuning range required the bias voltage or the capacitance (varactor diode, V_{R1}) to be varied from 4.9 V – 25.4 V or 3.28 pF – 0.74 pF, respectively [34]. Fig. 11 presents a comparison of the simulated and measured $|S_{11}|$ showing the frequency tuning of the first band, which are in good agreement.

Next, similar steps were performed for the remaining three frequency bands where the tuning ranges of these bands were investigated separately. For brevity only measured results of the second, third and fourth bands are discussed below. As shown in Fig. 12(a), the second frequency band was tuned from 1.17 GHz to 2.2 GHz by changing the bias voltage (V_2) of the second varactor V_{R2} from 5.6 V – 13.1 V, while the first, third, and fourth frequencies were fixed at 0.83 GHz, 2.4 GHz and 3.4 GHz, respectively. Next, to investigate the independent tunability of the third band, the bias voltages of the first, second and fourth varactors (V_{R1}, V_{R2} and V_{R4}) were kept constant while the third bias voltage (V_3) was varied. The measured $|S_{11}|$ results presented in Fig. 12(b) shows the frequency tuning of the frequency band, which

III. ANTENNA PROTOTYPE
The final design of the antenna was manufactured on Rogers TMM4 substrate (1.524 mm thick and 0.5 oz. copper coating) with the ground plane measuring 100 mm × 50 mm. Fig. 10 shows pictures of the top and bottom layers of the manufactured prototype antenna with all the biasing components present. Although, the actual antenna size is 21.65 mm × 50 mm, the ground plane is extended to emulate the form factor of a handheld mobile device's PCB.

The biasing circuit was also integrated on the same PCB, which was manufactured using a standard etching process. Next, the additional components such as varactor diodes, RF-chokes, capacitors (etc.) were soldered to complete the prototype antenna as per the schematic diagram depicted in Fig. 9. The RF-DC isolation was attained using the RF choke TCCH-80+ (Mini-circuits), which has an inductance of ≈4.0 μH and was selected mainly because of: very broadband operating frequency, 50 MHz-8200 MHz; very low parasitic capacitance, 0.1 pF; very low DC resistance of 0.1Ω; and insertion loss ranging from 0.5 dB - 1.1 dB [38]. Finally, the continuity, in circuit and isolation tests were performed

capacitor C_1 results in 1) shifting the resonant frequency of the first band towards a higher frequency and 2) creates an additional resonance (dual band) at around 2.2 GHz. It should be noted that the feed position is unchanged in this case and also when Var1 is located at 11.2 mm from the edge of the slot, the first resonance is mismatched while the resonance created at 2.2 GHz shows a good impedance match. This additional resonance also affects the third band (2.4 GHz), which completely loses its impedance matching. Overall, it is observed that for any changes made in the varactor's location, the feed position must also be adjusted to obtain a good impedance match, as reported in [36], [37].

TABLE 2. Tuning ranges of the proposed antenna.

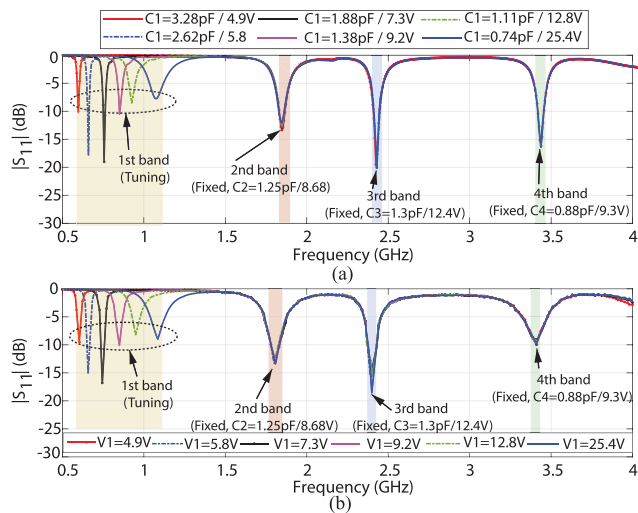| Slots / Varactors	Band 1	Band 2	Band 3	Band 4
Slot 1 *(Varactor 1)*	Tunable (0.6-1.17 GHz)	Fixed (1.85 GHz)	Fixed (2.4 GHz)	Fixed (3.4 GHz)
Bias voltage	$V_1 = 4.9$ - 25.4 V	$V_2 = 8.68$ V	$V_3 = 12.4$ V	$V_4 = 9.3$ V
Slot 2 *(Varactor 2)*	Fixed (830 MHz)	Tunable (1.17-2.2 GHz)	Fixed (2.4 MHz)	Fixed (3.4 GHz)
Bias voltage	$V_1 = 9.0$ V	$V_2 = 5.6$ - 13.1 V	$V_3 = 12.4$ V	$V_4 = 9.3$ V
Slot 3 *(Varactor 3)*	Fixed (830 MHz)	Fixed (1.85 GHz)	Tunable (2.2-2.7 GHz)	Fixed (3.4 GHz)
Bias voltage	$V_1 = 9.0$ V	$V_2 = 8.68$ V	$V_3 = 7.6$ - 27.5 V	$V_4 = 9.3$ V
Slot 4 *(Varactor 4)*	Fixed (830 MHz))	Fixed (1.85 GHz)	Fixed (2.4 GHz)	Tunable (2.6-3.6 GHz)
Bias voltage	$V_1 = 9.0$ V	$V_2 = 8.68$ V	$V_3 = 12.4$ V	$V_4 = 1.9$ -9.7 V
Tuning range (Total $\approx 142\%$)	$\approx 64\%$	$\approx 67\%$	$\approx 27\%$	$\approx 33\%$

FIGURE 11. The input reflection coefficients ($|S_{11}|$) showing the frequency tuning of the first band of the proposed quad-band antenna while the remaining three bands are unaffected. (a) Simulation and (b) Measured results.
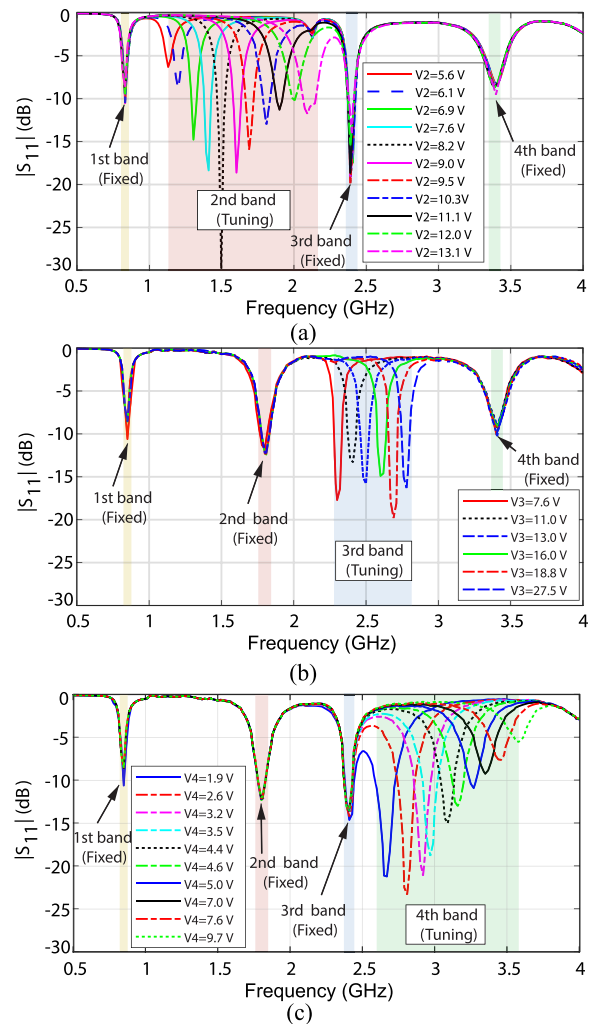

FIGURE 12. Measured input reflection coefficients ($|S_{11}|$) of the proposed antenna showing the independent tuning range of the (a) second band, (b) third band and (c) fourth band.

illustrates that the third band can be continuously tuned from 2.2 GHz to 2.7 GHz when V_3 is varied from 7.6 V $- 27.5$ V. Finally, the tunability of the fourth band was investigated by varying the fourth bias voltage, V_4, while keeping the first three bias voltages (V_1-V_3) fixed at 9.0 V, 8.68 V, and 12.4 V, respectively. As observed from Fig. 12(c), the first three bands are fixed at 0.83, 1.85, and 2.4 GHz, while the frequency of the fourth band is tuned from 2.6 GHz - 3.6 GHz when V_r is varied from 1.9 V to 9.7 V. A detail summary of the tunable range of each frequency band of the proposed antenna along with the bias voltage information is presented in Table 2.

Thus, it is demonstrated that each of the four bands of the proposed quad-band antenna can be independently tuned without affecting the remaining three bands. Besides, concurrent bands (two, three or all four) can also be tuned to a different frequency band when the respective reverse bias voltages are varied concurrently, as shown in Fig. 13. For example, Fig. 13(a) shows the frequency tuning of the first frequency band by changing the bias voltage (V_1) of the first varactor (V_{r1}) from 7.0 V $- 9.0$ V while the remaining three bands are fixed ($V_2 = 8.68$ V, $V_3 = 12.4$ V,

$V_4 = 9.3$ V). In Fig. 13(b), however, the first two bands are concurrently tuned by changing the bias voltages, V_1 and V_2, from 7.0 V and 8.2 V $- 9.0$ V and 5.0 V, respectively, while keeping the remaining two bands unchanged. Correspondingly, the concurrent tuning of the first three bands is shown in Fig. 13(c) and achieved by varying the first three bias voltages, V_1 to V_3, while V_4 was fixed. Finally, all four bands were
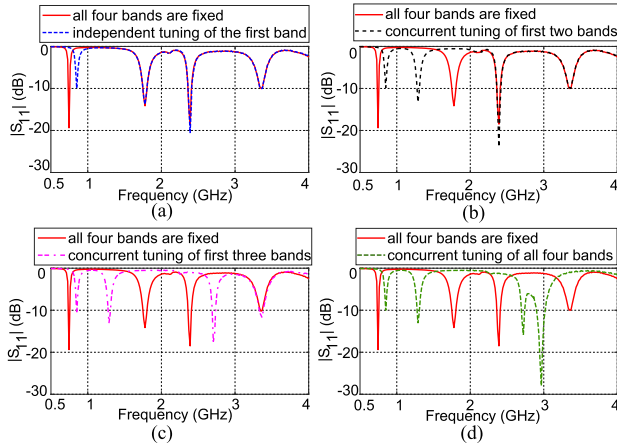
FIGURE 13. Measured reflection coefficients of the proposed quad-band antenna demonstrating (a) single band tuning, (b) concurrent tuning of the first two bands, (c) concurrent tuning of the first three bands, and (d) concurrent tuning of all the four bands.

concurrently tuned by changing all the four reverse bias voltages (V_1–V_4) as observed in Fig. 13(d). For brevity, only a single frequency band (in each of the four tunable bands) is switched in the aforementioned concurrent tuning example; however, it demonstrates the concept and confirms that the proposed antenna can achieve concurrent tuning.

B. RADIATION PATTERNS AND GAIN

The far-field radiation characteristics, including the radiation patterns and gain of the proposed antenna have been studied in simulation and measurements. During the experimental characterisation, the radiation patterns were measured at various frequency intervals across the entire 3 GHz tuning range (0.6 to 3.6 GHz), however, only a single frequency band in each of the four tuning bands is presented for brevity. The radiation pattern measurements were performed in a fully calibrated anechoic chamber using the NSI far-field Antenna Measurement System (800F-10). In addition to a Vector Network Analyser (Agilent E5071C) and a wideband horn antenna (HF 906), four DC power supplies (0-30V) were employed to provide the biasing voltages to the varactor-loaded slots. The horn antenna (transmitter) was adjusted for each operating frequency, in each of the four tuning bands, until maximum received power was recorded. In order to identify the E-plane, the antennas were rotated until the electric fields were matched and vertically polarised. Then, the antenna under test (AUT, quad-band), placed on the antenna positioner, was rotated azimuthally for measuring the cuts in the E-plane. For cross-polarised patterns, the AUT was rotated by 90°. The H-plane radiation pattern measurements were performed in a similar fashion.

The normalised radiation patterns for the co-polarisations and cross-polarisations in the $xz(H)-$ and $yz(E)-$planes measured at 850, 1800, 2400 and 3400 MHz are shown in Fig. 14(a-d). As desired for the mobile terminals (sub-6GHz 5G Radio Receivers), the proposed antenna has similar to omnidirectional radiation characteristics, which is
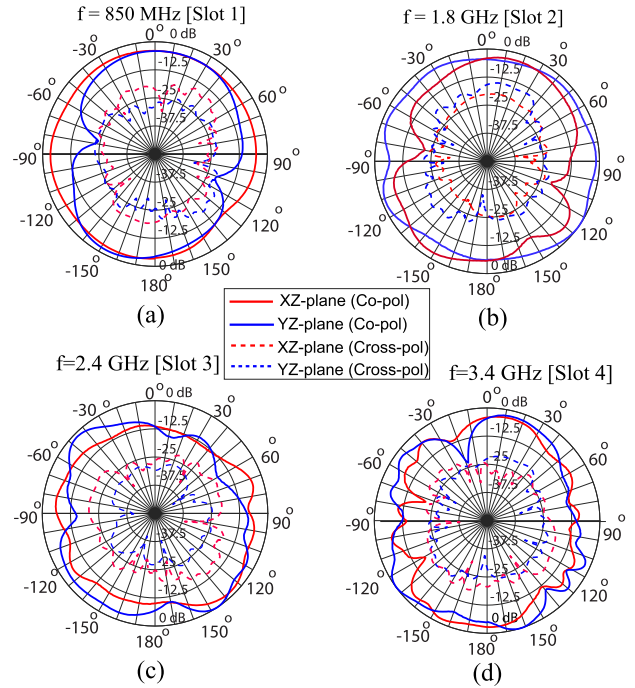

FIGURE 14. Normalised co- and cross-polarised radiation patterns of the prototype quad-band antenna in the *xz*- and *yz*-plane measured at (a) 850MHz, (b) 1800 MHz, (c) 2400 MHz and (d) 3400 MHz.
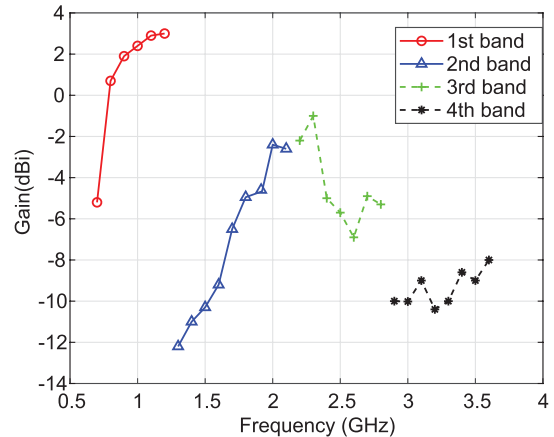

FIGURE 15. Measured gain of the antenna in each band (1-4).

advantageous for coverage purposes. It is important to mention that each loaded-slot (1-4) was appropriately biased at the time of pattern measurements. To minimize the unwanted radiations from the biasing lines, all the power supplies were kept outside the chamber and the wires were shielded and ferrite beads were used. Distortion and additional nulls can be observed in the radiation patterns at higher frequencies such as 2.4 GHz and 3.4 GHz, as shown in Fig. 14(c) and (d), which are attributed to the unwanted radiation and reflection from the feeding cables.

The gain of the antenna was measured using the gain comparison method using the same wideband Horn antenna (HF 906) in an anechoic chamber. Fig. 15 shows the mea-
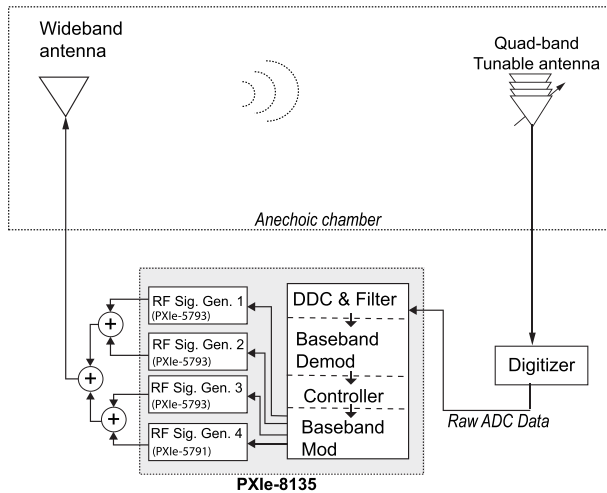
FIGURE 16. An illustration of the experimental setup of the test-bed used for the EVM measurements and to validate the proposed quad-band tunable antenna.

FIGURE 17. Measured EVM performance of (a) concurrent multiband and (b) individual bands for QPSK modulated single-carrier transmission over the quad-band testbed.

sured gain of the proposed antenna for each band. For the first band, the gain varies between -5 and 3 dBi, while in the second it varies between -12 and -2 dBi. Similarly, the gain measured in the third and fourth bands fluctuates between -2 and -5 dBi, and -10 and -8 dBi, respectively. The simulated efficiency of the proposed quad-band antenna varies in each tuning band and the maximum value was found to be $\approx 24\%$ at 780 MHz. The lossy varactor diodes are the main contributor of the low gain, which may be replaced by digitally tuned capacitors in our future work. A separate study also showed that by replacing the varactor diode with a fixed capacitor, an improvement of up to 4.5 dBi can be achieved at 0.6 GHz.

It is also observed that there are multiple nulls in the radiation patterns at the higher bands (Fig. 14(d)) and that the gain is also relatively low at these higher bands. While the extent of these mentioned characteristics for 5G is not fully studied, it is shown through the system level analysis that the proposed antenna (with the given parameters) in a mobile terminal's receiver provides a suitable isolation for concurrent channels using a single chain receiver (Section IV-C).

C. ERROR VECTOR MAGNITUDE PERFORMANCE

The performance of the proposed quad-band antenna is tested using a tunable, concurrent, quad-band, direct RF digitization and single chain radio receiver 5G testbed. Fig. 16 represents the test-bed schematically. The controller (PXIe-8135) is a PC running LabVIEW and LabVIEW communications suite with LTE Application Framework, where the digital frequency translation and baseband processing take place. Four independent QPSK or QAM modulated signals are generated at the controller and passed to the RF signal generators (PXIe-5793) and the transceiver (PXIe-5791). The generated signals are then combined (ZAPD-2-272-S+) and transmitted through a wideband antenna (UHALP-9108A).
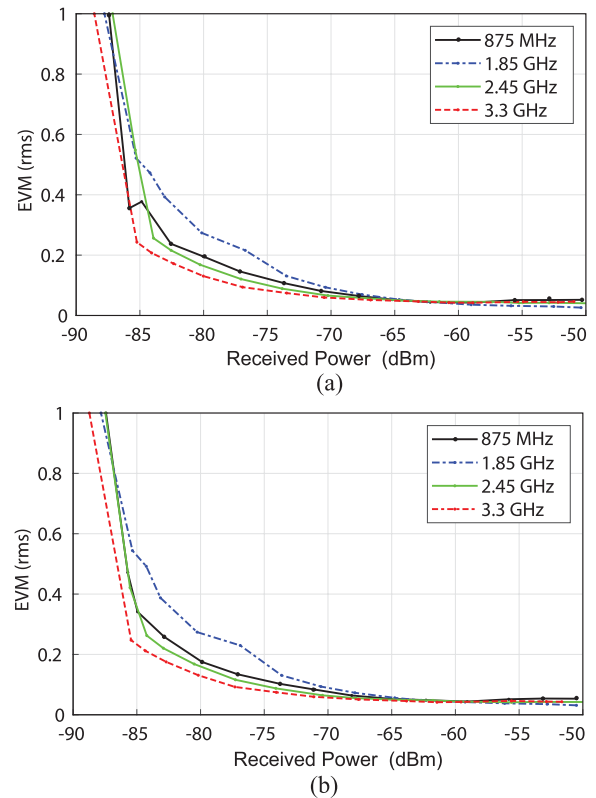
The RF digitizing single chain receiver is comprised of the proposed quad-band antenna, a digital acquisition oscilloscope (WaveRunner 8404) as digitizer, a quad-band DDC and the basedband processors. The digital oscilloscope has built in LNAs, but if more amplification was needed, additional LNAs can be used in the receiver chain. More information regarding the test-bed is provided in [21].

In order to analyse the isolation of each band on a system level, the inter-band interference (IBI) was investigated by measuring the error vector magnitude (EVM) performance. Four independent QPSK modulated single-carrier signals centred at 875 MHz, 1.85, 2.45 and 3.3 GHz were transmitted, received and the EVM was measured. The maximum signal bandwidth according to LTE standards from tables 5.5-1 and 5.6.1-1 of 3GPP TS 36.101 standard [39] was chosen for each band. Therefore, a signal with 15 MHz bandwidth was used for 875 MHz band and signals with 20 MHz bandwidth were used for 1.85, 2.45 and 3.3 GHz bands.

EVM versus received signal power for the four processed signals in concurrent transmission mode is shown in Fig. 17(a). For -70 dBm to -50 dBm received input power, the EVM performance for all the bands is almost similar and below 10%, which is negligible and no data transmission error was encountered. For QPSK modulation, up to approximately 20% EVM performance is acceptable. Therefore, for -75 dBm received input power and above, acceptable performance for all the bands is achieved.

TABLE 3. Comparison of the proposed antenna with previously reported reconfigurable antennas.

Ref.	Freq. range (GHz)	Number of Bands	Size (W×L×H mm³)	Tuning ratio	Gain (dBi)
[18]	0.8-1 & 1.7-2.4	Dual	40×18 ×7	N/A (fixed)	-1.1 to 3.4
[19]	1.1-2.94	Dual	110×115 ×0.5	2.67:1	1.7 to 2.1
[20]	0.42-1.48	Single	20×35 ×7	3.52:1	-0.4
[17]	2.6-3.35	Single	77×57 ×7	1.28:1	Not reported
[21]	0.61-2.7	Three	17×50 ×1.86	4.42:1	-5.8 to 0.3
[22]	1.3-1.4 & 1.7-5.2	Single (2×2 MIMO)	60×100 ×1.56	1.13:1 & 3:1	4.5
This work	0.6-3.6	Four	21.65×50 ×1.52	6:1	-12 to 3

For −75 dBm and lower input power levels, the performance is reduced and EVM grows over 20% and there is total distortion near −90 dBm.

In order to analyse the mutual interference between the received signal bands, the EVM performance for the same QPSK signals when transmitted individually was measured and the results are presented in Fig. 17(b). The curves for concurrently measured bands for received input power levels above −80 dBm are almost identical to those for the individually measured bands, which are represented in Fig. 17(a). For power levels below −80 dBm they have similar trends in performance degradation. Hence, in concurrent transmission mode, the effect of the mutual coupling between bands is negligible and the EVM performance of concurrent and individual transmission modes is similar.

V. DISCUSSION

There are some limitations of this work, which are described here. The four tunable bands (i.e. 1st, 2nd, 3rd and 4th) comprise of bands that are quite narrow (e.g., 20 MHz), as shown in Fig. 11 and 12. However, the tunable ranges of each band is considerably large and the overall bandwidths attained by these narrow bands in the 1st, 2nd, 3rd and 4th bands are 64%, 67%, 27% and 33% (approximately), respectively. Whilst the operational bandwidth of each of the four separate bands are fairly large, any practical applications that deploy the prototype antenna are nevertheless restricted to a bandwidth of a few percent of the tuned centre frequencies, which varies from 5 MHz to 160 MHz (approximately). In spite of this mentioned limitation, the proposed antenna has sufficient operating bandwidth(s) for many wireless systems as demonstrated for 20 MHz LTE channels in Section IV-C.

Moreover, it is observed that for two contiguous frequency bands, when tuned towards each other, a wideband behaviour is achieved. For example, a bandwidth of ≈340 MHz is obtained when the third and fourth bands are brought closer to each other, as shown in Fig. 13(d). This arrangement could advantageously benefit carrier aggregation in 5G radios.

In this work, −6 dB matching ($|S_{11}|$) is considered sufficient (Fig(s). 11 and 12) as the prototype antenna is proposed for a mobile terminal or user equipment (UE) where the transceiver power levels are relatively much lower and hence the effects of reflections from a UE antenna on the mobile receiver hardware would be acceptable. It should be mentioned that an input reflection coefficient of −6 dB (of an antenna) would result in 25% of reflected power and 75% would be received by the antenna.

A comparison of the proposed work with the state-of-the-art tuning antennas is presented in Table 3. The proposed work has a distinct advantage over previously reported works as it offers a much wider tunable bandwidth, which is achieved by suppressing the higher-order resonant modes. Overall, this antenna offer four independently-controlled tunable bands, covering a very wide frequency range, that can be used for sub-6GHz 5G concurrent communication.

VI. CONCLUSION

In this paper, a low-profile quad-band frequency agile antenna is presented for a tunable, concurrent, quad-band single chain radio receiver for 5G New Radio (NR). The proposed antenna employs four slots to produce four distinct resonances, which are tuned electronically using varactor diodes. The orientation of the four slots were exploited to achieve a compact design and to enable their excitation using a single microstrip feedline–without any additional impedance matching network. The simulation and measured results of the antenna were in good agreement. All of the four bands demonstrated their own tuning ranges (64%, 66%, 27% and 33%), covering frequencies from 600 MHz to 3600 MHz and a combined frequency tuning range of ≈143%. Furthermore, concurrent frequency tuning of two, three and all four bands was demonstrated. Following the measurement of the radiation patterns and gain, the antenna was evaluated (using over-the-air testbed) in a tunable, concurrent, quad-band single chain radio receiver for 5G NR. The system level performance of the proposed antenna in a mobile receiver was investigated and negligible error vector magnitude demonstrated good isolation between the concurrent bands.

REFERENCES

[1] W. Guo and T. O'Farrell, "Capacity-energy-cost tradeoff in small cell networks," in *Proc. IEEE 75th Veh. Technol. Conf. (VTC Spring)*, Yokohama, Japan, May 2012, pp. 1–5.

[2] P. Marsch, I. Da Silva, O. Bulakci, M. Tesanovic, S. E. El Ayoubi, T. Rosowski, A. Kaloxylos, and M. Boldi, "5G radio access network architecture: Design guidelines and key considerations," *IEEE Commun. Mag.*, vol. 54, no. 11, pp. 24–32, Nov. 2016.

[3] R. E. Hattachi and J. Erfanian, "NGMN (Next Generation Mobile Networks Alliance) 5G white paper," Next Gener. Mobile Netw. Alliance, Reading, U.K., Tech. Rep. version 1, Feb. 2015.

[4] R. Singh, Q. Bai, T. O'Farrell, K. L. Ford, and R. J. Langley, "Demonstration of RF digitising concurrent dual-band receiver for carrier aggregation over TV white spaces," in *Proc. IEEE 84th Veh. Technol. Conf.*, Montreal, QC, Canada, Sep. 2016, pp. 1–5.

[5] R. Singh, Q. Bai, T. O'Farrell, K. L. Ford, and R. J. Langley "Concurrent, tunable, multi-band, single chain radio receivers for 5G RANs," in *Proc. IEEE 85th Veh. Technol. Conf. (VTC Spring)*, Sydney, NSW, Australia, Jun. 2017, pp. 1–5.

[6] A. Petosa, *Frequency-Agile Antennas for Wireless Communications*. Norwood, MA, USA: Artech House, Nov. 2013.

[7] A. Petosa, "An overview of tuning techniques for frequency-agile antennas," *IEEE Antennas Propag. Mag.*, vol. 54, no. 5, pp. 271–296, Oct. 2012.

[8] C. G. Christodoulou, Y. Tawk, S. A. Lane, and S. R. Erwin, "Reconfigurable antennas for wireless and space applications," *Proc. IEEE*, vol. 100, no. 7, pp. 2250–2261, Jul. 2012.

[9] S. Asif, A. Iftikhar, M. N. Rafiq, B. D. Braaten, M. S. Khan, D. E. Anagnostou, and T. S. Teeslink, "A compact multiband microstrip patch antenna with U-shaped parasitic elements," in *Proc. IEEE Int. Symp. Antenna Propag.*, Vancouver, BC, Canada, Jul. 2015, pp. 617–618.

[10] D. E. Anagnostou and A. A. Gheethan, "A coplanar reconfigurable folded slot antenna without bias network for WLAN applications," *IEEE Antennas Wireless Propag. Lett.*, vol. 8, pp. 1057–1060, 2009.

[11] H. F. Abutarboush, "A reconfigurable wideband and multiband antenna using dual-patch elements for compact wireless devices," *IEEE Trans. Antennas Propag.*, vol. 60, no. 1, pp. 36–43, Jan. 2012.

[12] A. C. K. Mak, C. R. Rowell, R. D. Murch, and C.-L. Mak, "Reconfigurable multiband antenna designs for wireless communication devices," *IEEE Trans. Antennas Propag.*, vol. 55, no. 7, pp. 1919–1928, Jul. 2007.

[13] S. M. Asif, A. Iftikhar, S. M. Khan, M. Usman, and B. D. Braaten, "An E-shaped microstrip patch antenna for reconfigurable dual-band operation," *Microw. Opt. Technnol. Lett.*, vol. 58, no. 6, pp. 1485–1490, Jun. 2016.

[14] M. S. Khan, S. Asif, A.-D. Capobianco, B. Ijaz, D. E. Anagnostou, and B. D. Braaten, "Frequency reconfigurable self-adapting conformal array for changing surfaces," *IET Microw., Antennas Propag.*, vol. 10, no. 8, pp. 897–907, Jun. 2016.

[15] D. Peroulis, K. Sarabandi, and L. P. B. Katehi, "Design of reconfigurable slot antennas," *IEEE Trans. Antennas Propag.*, vol. 53, no. 2, pp. 645–654, Feb. 2005.

[16] N. Behdad and K. Sarabandi, "A wide-band slot antenna design employing a fictitious short circuit concept," *IEEE Trans. Antennas Propag.*, vol. 53, no. 1, pp. 475–482, Jan. 2005.

[17] S.-L. S. Yang, A. A. Kishk, and K.-F. Lee, "Frequency reconfigurable U-slot microstrip patch antenna," *IEEE Antennas Wireless Propag. Lett.*, vol. 7, pp. 127–129, May 2008.

[18] S. H. Lee, Y. Lim, Y. J. Yoon, C.-B. Hong, and H.-I. Kim, "Multiband folded slot antenna with reduced hand effect for handsets," *IEEE Antennas Wireless Propag. Lett.*, vol. 9, pp. 674–677, 2010.

[19] N. Behdad and K. Sarabandi, "Dual-band reconfigurable antenna with a very wide tunability range," *IEEE Trans. Antennas Propag.*, vol. 54, no. 2, pp. 409–416, Feb. 2006.

[20] H. Li, J. Xiong, Y. Yu, and S. He, "A simple compact reconfigurable slot antenna with a very wide tuning range," *IEEE Trans. Antennas Propag.*, vol. 58, no. 11, pp. 3725–3728, Nov. 2010.

[21] Q. Bai, R. Singh, K. L. Ford, T. O'Farrell, and R. J. Langley, "An independently tunable tri-band antenna design for concurrent multiband single chain radio receivers," *IEEE Trans. Antennas Propag.*, vol. 65, no. 12, pp. 6290–6297, Dec. 2017.

[22] R. Hussain, M. S. Sharawi, and A. Shamim, "4-element concentric pentagonal slot-line-based ultra-wide tuning frequency reconfigurable MIMO antenna system," *IEEE Trans. Antennas Propag.*, vol. 66, no. 8, pp. 4282–4287, Aug. 2018.

[23] H. F. Abutarboush, R. Nilavalan, S. W. Cheung, and K. M. Nasr, "Compact printed multiband antenna with independent setting suitable for fixed and reconfigurable wireless communication systems," *IEEE Trans. Antennas Propag.*, vol. 60, no. 8, pp. 3867–3874, Aug. 2012.

[24] C. T. P. Song, Z. H. Hu, J. Kelly, P. S. Hall, and P. Gardner, "Wide tunable dual-band reconfigurable antenna for future wireless devices," in *Proc. Loughborough Antennas Propag. Conf.*, Loughborough, U.K., Nov. 2009, pp. 601–604.

[25] S. N. Islam, "Design of a compact quad-band antenna with independent frequency tuning," *Electron. Lett.*, vol. 54, no. 15, pp. 920–922, Jul. 2018.

[26] C. A. Balanis, *Antenna Theory: Analysis and Design*, 4th ed. Hoboken, NJ, USA: Wiley, 2016.

[27] R. Garg, *Microstrip Antenna Design Handbook*. Norwood, MA, USA: Artech House, 2001.

[28] R. Garg, *Microstrip Lines Slotlines*, 3rd ed. Norwood, MA, USA: Artech House, 2013.

[29] D. M. Pozar, *Microwave Engineering*, 4th ed. Hoboken, NJ, USA: Wiley, 2016.

[30] N. Behdad and K. Sarabandi, "A varactor-tuned dual band slot antenna," *IEEE Trans. Antennas Propag.*, vol. 54, no. 2, pp. 401–408, Feb. 2006.

[31] G. Matthaei, E. M. T. Jones, L. Young, *Microwave Filters, Impedance-matching Networks, and Coupling Structures*. Norwood, MA, USA: Artech House, 1980.

[32] H. Lee, "Independently tunable low-profile dual-band high-impedance surface antenna system for applications for UHF band," *IEEE Trans. Antennas Propag.*, vol. 60, no. 9, pp. 4092–4101, Sep. 2012.

[33] C. Mias and J. Yap, "A Varactor-tunable high impedance surface with a resistive-lumped-element biasing grid," *IEEE Trans. Antennas Propag.*, vol. 55, no. 7, pp. 1955–1962, Jul. 2012.

[34] Infineon Technologies. (May 10,2018). *Silicon Tuning Diodes*. [Online]. Available: http://www.infineon.com/cms/en/product/rf-wireless-control/rf-diode

[35] Skyworks. (Mar. 1, 2018). *SMV 1405 Series, Plastic Abrupt Junction Tuning Varactor*. [Online]. Available: http://www.skyworksinc.com/Product/552/SMV1405

[36] B. Das and K. Joshi, "Impedance of a radiating slot in the ground plane of a microstripline," *IEEE Trans. Antennas Propag.*, vol. AP-30, no. 5, pp. 922–926, Sep. 1982.

[37] J. P. Kim and W. S. Park, "Network modeling of an inclined and off-center microstrip-fed slot antenna," *IEEE Trans. Antennas Propag.*, vol. 46, no. 8, pp. 1182–1188, Aug. 1998.

[38] Mini-Circuits. (Jun. 2, 2018). *Surface Mount RF Chokes*. [Online]. Available: https://www.minicircuits.com/WebStore/rfchokes.html

[39] *LTE; User Equipment (UE) Radio Transmission and Reception*, document ETSI TS 36.101, version 14.3.0, 3GPP, Apr. 2017.

SAJID M. ASIF received the M.S. degree in radio frequency communication engineering from the University of Bradford, U.K., in 2006, and the Ph.D. degree in electrical and computer engineering from North Dakota State University (NDSU), Fargo, ND, USA, in 2017.

He is currently a Research Associate in frequency agile radio with The University of Sheffield, U.K. He has authored or coauthored more than 59 peer-reviewed journal and conference papers. His research interests include RF/microwave circuits, printed antennas, implantable antennas, wireless sensors, and energy harvesting for biomedical applications. Dr. Asif is affiliated with the electrical engineering honor society, IEEE-Eta Kappa Nu; engineering honor society, Tau Beta Pi; and the professional organization, IEEE. He has received numerous awards and scholarships, including the internationally prestigious IEEE-AP-S Doctoral Research Grant, in 2015; the NSF funded ND-EPSCOR Doctoral Dissertation Assistantship Award, from 2005 to 2016; and the First-Place in the NDSU Innovation Challenge Competition, in 2017. He served the IEEE Red River Valley Section as the Chair (Y 2015) and the Vice-Chair (Y 2014).

MOHAMMAD R. ANBIYAEI received the M.Sc. (Hons.) and Ph.D. degrees from the Electronic and Electrical Engineering Department, The University of Sheffield, in 2012 and 2018, respectively. He was a Research Associate with the Electronic and Electrical Engineering Department, The University of Sheffield, from April 2018 until March 2019. He is currently a Postdoctoral Research Fellow with the Faculty of Engineering, Alzahra University, Tehran, Iran. His current research interests include anomaly detection of communication systems using machine learning and AI, software defined radio, reconfigurable concurrent multiband transceivers, and array signal processing.

KENNETH L. FORD received the B.Eng. and Ph.D. degrees in electronic engineering from The University of Sheffield, Sheffield, U.K., in 1998 and 2003, respectively. In 2001, he joined the Stealth Materials Department, Advanced Technology Centre, BAE SYSTEMS, Towcester, U.K., before returning to The University of Sheffield, in 2005 as a Lecturer of communications. He was promoted to Senior Lecturer, in 2012, Reader, in 2019, and Professor, in 2020. His research interests include reconfigurable antennas, miniaturized antennas, metamaterials, and electromagnetic structures for biomedical applications.

TIMOTHY O'FARRELL is currently the Chair Professor in wireless communications with The University of Sheffield, U.K. He is an Expert in wireless communication systems specializing in physical layer signal processing, radio resource management, and wireless network planning. He has pioneered research on energy efficient mobile cellular communications, the mathematical modeling of CSMA-based MAC protocols for WiFi, iterative block coding for wireless communication systems and spreading sequence design for CDMA wireless networks. He is an entrepreneur, being the cofounder and CTO of Supergold Communication Limited, from 1997 to 2007, a start-up that participated in the standardization of IEEE 802.11g with the MBCK proposal. In the framework of Mobile VCE (mVCE), he was the Academic Coordinator of the Core 5 Green Radio project, from 2009 to 2012, and a Leader in establishing energy efficiency as a global research field in wireless communications systems. He has managed 24 major research projects as a Principal Investigator. His current EPSRC project portfolio as PI includes the SERAN, and FARAD and DDmmMami projects. He has published 313 journal and conference papers, book chapters, patents, and technical reports. He has participated in standards, consultancy, and expert witness activities within the wireless sector.

Prof. O'Farrell is leading the U.K. Research Strategy Community Organization in Communications, Mobile Computing, and Networking within the EPSRC portfolio. He is the Director of the mVCE, a Chartered Engineer, and an IET Member.

RICHARD J. LANGLEY received the B.Sc. and Ph.D. degrees from the University of Kent, U.K.

After spending some time working on communications satellites at Marconi Space Systems in the 1970s, he became a Lecturer at the University of Kent, in 1979. He is currently the Head of the Communications Research Group, The University of Sheffield. He has published over 400 articles in international journals and conferences. His main research is in the fields of automotive antennas, propagation in the built environment, frequency selective surfaces, electromagnetic band gap materials and applications, multifunction antenna systems, and reconfigurable antennas. He initiated the setting up of the Wireless Friendly Building Forum, in 2009 to address the problems of wireless signal propagation in buildings and the built environment. He was promoted to a Personal Chair in antenna systems, in 1994. He is a past Chair of the *IET Antennas and Propagation Professional Network*. He was an Honorary Editor of *IEE Proceedings—Microwaves, Antennas and Propagation*, from 1995 to 2003. In 1997, he founded the European Technology Centre for Harada Industries Japan, the world's largest supplier of automotive antennas. The center researches and develops advanced hidden antenna systems for the global automotive market including radio, telephone and navigation systems. After successfully building up the technology and business he rejoined academic life, in 2003.

• • •